Journal of Alloys and Compounds 771 (2019) 246–253

Contents lists available at ScienceDirect

Journal of Alloys and Compounds

journal homepage: http://www.elsevier.com/locate/jalcom

Selenization of electrochemically synthesized copper-indium layers from non-aqueous solution for solar cell application

Priyanka U. Londhe, Ashwini B. Rohom, Nandu B. Chaure*

Department of Physics, Savitribai Phule Pune University (formerly University of Pune), Pune, 411007, India

ARTICLE INFO

Article history:
Received 8 February 2018
Received in revised form
22 August 2018
Accepted 27 August 2018
Available online 30 August 2018

Keywords:
Electrodeposition
Nucleation
Selenization
$CuInSe_2$
Thin film solar cells

ABSTRACT

A simple two-step, electrodeposition of copper-indium (Cu-In) intermetallic alloy thin films followed by selenization process was employed for the synthesis and development of $CuInSe_2$ (CIS) thin film solar cells (TFSC). The co-deposition of Cu and In in ethylene glycol at 130 °C was studied using the cyclic voltammetry (CV) to obtain a stable Cu-In phase. A wide window of deposition potentials from −0.7 V to −1.5 V versus Ag/AgCl reference electrode was optimized. Three different potentials, −0.7 V, −1.0 V and −1.3 V are chosen to deposit the Cu-In intermetallic alloy thin films, which were further selenized in controlled selenium ambient at 400 °C. The selenization effect is studied extensively on structural, morphological, optical and compositional properties of selenized Cu-In (CIS) thin films. Polycrystalline CIS layers with tetragonal crystal structure are obtained upon selenization of Cu-In thin films. Three prominent reflections of CIS, (112), (204/220) and (312/116) are exhibited in all selenized Cu-In layers. Additional secondary phases of Cu_xSe_{1-x} are attributed for the layers grown at −0.7 and −1.0 V. Compact and void-free surface morphology with particle size ~1–2 μm was observed for all selenized samples. The selenized Cu-In layer sample deposited at −1.3 V measure ~1.06 eV energy band gap with polycrystalline tetragonal chalcopyrite crystal structure of CIS. The photoelectrochemical measurement confirms the growth of p-type material. A selenized Cu-In layer deposited at −1.3 V with CdS window layer measured power conversion efficiency 5.44%.

1. Introduction

Energy concern is becoming more serious issue because of the global warming and diminutions of fossil fuels. This calls the research into green and renewable energy generation from natural resources, like sun, hydro and wind. Among all the energy sources, solar energy is very optimistic through abundant and clean energy. Presently, a crystalline Si-solar (c-Si) cell dominates the photovoltaic (PV) market [1]. However, the indirect band gap, low absorption coefficient, purity, processing steps involved for c-Si solar cell leads to the high production cost [2]. In contrast, CIGS [3,4], CdTe [5,6] and a-Si:H [7], second generation thin film solar cells (TFSC), are the promising alternative to c-Si due to its direct band gap, easy availability of materials, low processing cost and high absorption coefficient. 22.8%, record value efficiency is accomplished for CIGS TFSC which can be increased up to 25% closer to the C-Si technology [8].

CIS based materials from chalcopyrite family are environmental friendly with suitable properties for the development of high efficiency solar cells. Till date the highest efficient (22.8%) CIGS TFSC is developed by using the co-evaporation technique [4]. However, the instrumentation, production cost and large material utilization, slow growth rate promotes to develop the new cheap vacuum-free deposition methods. Furthermore, the vacuum based methods are not suitable over large area solar cells due to the inhomogeneous deposition [9,10]. Various low-cost, non-vacuum solution based methods have been employed for the deposition of CIS. Among all, the electrodeposition is one of the most suitable methods for large area device production, with over 95% utilization of the materials and high growth rate [11–13].

Two different ways are generally adopted for the electrodeposition of CIS thin films. A co-deposition of all precursors in a single bath [14] and two-step process involving Cu-In/Cu-In-Ga co-deposition followed by selenization/sulfurization [15,16]. Additives and/or complexing agents are required for the co-deposition of different precursors in single bath [17–19], which could be the source of impurities in the deposit. A high crystalline absorber layer

* Corresponding author.
E-mail address: n.chaure@physics.unipune.ac.in (N.B. Chaure).

https://doi.org/10.1016/j.jallcom.2018.08.264
0925-8388/

without undesired phases, large grains with uniform homogeneous growth are the key factor for the development of high efficiency TFSC device. The post-deposition heat treatment of absorber layers at high temperature in presence of reactive gases (H_2Se, H_2S or vaporizes S/Se) is the proper procedure to obtain dense, well-crystallized layers suitable for photovoltaic devices. Here, we employed a two-step process for CIS deposition due to the wide differences in the reduction potentials of Cu, In and Se.

Some reports are available on the deposition of Cu-In thin films from aqueous medium as well as its nanoparticles. Cu-In nano particles are synthesized with melt atomization technique with 10.5% efficiency by Norswaorthy et al. [20]. Kind et al., in 2011 synthesized citrate capped $Cu_{11}In_9$ nanoparticles by polyol method and fabricated solar cell with 7% efficiency [21]. Prosini et al. reported the electrodeposition of Cu-In thin films onto different substrates [22]. Electrodeposited Cu-In layers were sulfurized to obtain the $CuInS_2$ thin films by Herrero et al. [23]. Cummings et al. reported the selenization of Cu-In alloy deposited by rotating disc electrodeposition [24].

In the present study we have reported the electrodeposition of Cu-In layers from non-aqueous bath at higher working temperature (130 °C), followed by selenization. In electrochemical deposition the most common approach to the growth of metal, oxide and semiconductor thin film is from the aqueous bath, however, H^+ reduction results the poor crystalline, non-adhesive, non-uniform and inhomogeneous layers [24,25], which further limit the electrochemical window. The ionic liquids and non-aqueous can be resolved the above issues. The ionic liquids have to be utilized in the inert ambient due to its hygroscopic nature [26]. However, the non-aqueous electrolytes have several advantages, such as wider electrochemical window, absence of hydrogen evolution and the growth of the material can be performed at higher temperature due to the high boiling point. Due to the availability of large number of non-aqueous solvents, there is the feasibility to choose an appropriate solvent. Further, most of the inorganic compounds are soluble in non-aqueous solvent, therefore, there is also a feasibility to choose additives and complexing agents. The higher working temperature supports the growth of highly crystalline and large particle size layers [27]. With and without selenized Cu-In samples were characterized with the range of characterization techniques to study the different properties and solar cell devices were prepared.

2. Experimental

Two-step method was employed for CIS formation/deposition. Firstly, the Cu-In layers were electrodeposited from ethylene glycol bath and subsequently selenized in a controlled selenium atmosphere.

2.1. Electrodeposition of Cu-In thin films

Copper chloride ($CuCl_2$, Sigma Aldrich - 99.9%) and Indium chloride ($InCl_3$, Sigma Aldrich - 99.9%) were used as Cu and In ion precursors for the deposition of Cu-In layers. Lithium Chloride (LiCl, Sigma Aldrich - 99.5%) was used as supporting electrolyte. Ethylene glycol (EG) was used as an electrolyte. Electrochemical mechanism of Cu-In growth was studied using cyclic voltammetry (CV) measurements. Biologic potentiostat/galvanostat model SP150 was used for the deposition of Cu-In layers potentiostatically onto fluorine doped tin oxide (FTO) (Pilkington, UK, 10–15 Ω/□) coated glass substrates at 130 °C. A standard three-electrode geometry with Ag/AgCl as reference, FTO as working and graphite as counter electrode were used for electrodeposition. A wide potential range from −0.7 V to −1.6 V versus Ag/AgCl was optimized from CV measurement. Chronoamperometric measurements were performed for different potentials. The properties of Cu-In layers were analyzed with various characterization techniques.

2.2. Selenization of Cu-In thin films

Cu-In layers electrodeposited at various deposition potentials were selenized in controlled atmosphere. Fig. 1 shows a schematic diagram of the selenization chamber. Two different selenization procedures are commonly used; one is the use of H_2Se gas [28] and another is generating the Se vapors from solid selenium ingots [29]. Our approach was the vaporization of Se ingots in a controlled ambient. The Se ingots were placed in an air tight graphite box. The graphite box consisting Cu-In layers and Se ingots were placed in the quartz tube with vacuum ~5×10^{-2} Torr. The heat treatment was carried out in to two-steps; firstly, the whole assembly was heated at 200 C for 15 min and subsequently the temperature of the system was raised up to 400 °C with heating rate 50 °C/s. The samples cooled to room temperature naturally. The diffusion of Se into grain boundaries is expected upon annealing at lower temperature (200 °C) and at second stage the Se react with of Cu-In alloy to produce a homogeneous CIS layer.

2.3. Electrochemical measurements

Cyclic voltammetric measurements were performed using Biologic potentiostat/galvanostat model SP 150. The conductivity type of selenized Cu-In layers (CIS) was studied by using photoelectrochemical (PEC) analysis. Three-electrode geometry was employed for PEC studies with graphite and Ag/AgCl as counter and reference electrode, respectively in 1 M KCl solution. A white light source of intensity 10 mW/cm^2 was used to illuminate the sample during the PEC measurements. The impedance spectroscopic

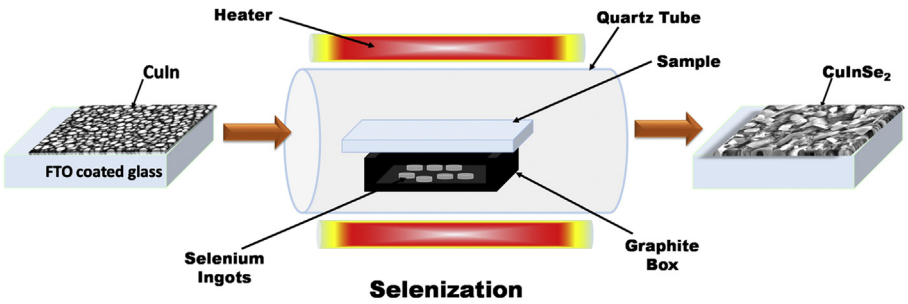

Fig. 1. A Schematic diagram of home-made selenization chamber.

measurements were performed for a frequency range, 1 MHz–100 mHz in 1 M NaCl solution.

2.4. Materials characterization

The structural properties were studied by using X-ray diffractometer, model Bruker D8 with Cu Kα anode of wavelength 0.154 nm. Surface topography of Cu-In and CIS layer was recorded with scanning electron microscope (SEM), JEOL JSM 6360 A, at operating voltage 20 kV. An elemental atomic percentage concentration was determined with the help of energy dispersive X-ray analysis (EDAX) technique attached with SEM equipment. Optical absorption measurements were performed with JASCO UV–Vis–NIR spectrophotometer, model-770. The optoelectronic properties were measured under dark and illuminated condition by using the solar simulator with input power intensity, 100 mW/cm^2.

2.5. Solar cell development

Superstrate solar cell structure, FTO/CdS/Selenized Cu-In/Au was prepared; wherein a Cu-In layer was electrodeposited at −1.3 V. CdS layers were prepared by chemical bath deposition technique [30]. Au-metal contact of diameter 3 mm was made by thermal evaporation technique at vacuum ~5×10^{-5} Torr. Prior to Au-metal contact the samples were etched in Br-Methanol and NaCN solution for 30 s each.

3. Results and discussion

3.1. Results obtained for Cu-In thin films

The electrochemical performance of Cu-In system in ethylene glycol and co-deposition potentials were optimized by using cyclic voltammetric measurements. Fig. 2 represents the cyclic voltammogram recorded for Cu-In system in ethylene glycol at working temperature 130 °C with scan rate 10 mV/s. A gradual rise in current noticed beyond ~ +0.37 V for the cathodic scan could be associated to the reduction of copper by following half electrode reaction (1) [31];

$$Cu^{2+} + 2e^- \rightarrow Cu \ldots\ldots\ldots\ldots\ldots\ldots E_o = +0.34\ \text{V versus SCE} \quad (1)$$

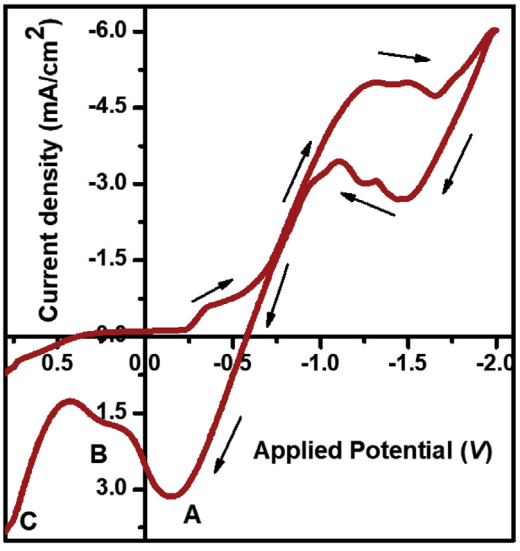

Fig. 2. Cyclic voltammogram recorded in an ethylene glycol electrolyte for Cu-In alloy, with 10 mV/s scan rate verses Ag/AgCl reference electrode at temperature 130 °C.

Further the cathodic current increased from −0.23 V is proposed due to the growth of Cu-rich, Cu-In intermetallic layers. The shift in the reduction potentials from the standard value is due to the change in open circuit potential, which depends upon various growth parameters, like nucleation, the concentrations of precursors, temperature of the bath, agitation conditions, position of the electrodes, etc.

The sharp rise in the cathodic current beyond −0.65 V is associated to the deposition of In-rich Cu-In thin films by the following charge transfer reaction;

$$In^{3+} + 3e^- \rightarrow In \ldots\ldots\ldots\ldots\ldots E_o = -0.34\ \text{V versus SCE} \ldots\ldots\ldots\ldots\ldots\ldots\ldots\ldots (2)$$

A plateau region observed from −1.10 to −1.50 V is proposed for the co-deposition of Cu and In. A plateau region attributed during reverse scan (anodic) from −1.5 V to-1.0 V is due to the deposition of Cu-In intermetallic layer on to low resistive layer deposited at high cathodic potentials (<-1.5 V). The stripping peak A, B and C attributed during reverse scan are associated to the oxidation of In-rich and Cu-rich phases of Cu-In thin film. Three different potentials, −0.7 V, −1.0 V and −1.5 V were chosen from cyclic voltammogram to grow Cu-In thin films.

The nucleation mechanism of Cu-In layers grown for different growth potentials was studied with the help of Scharifker and Hill's model [32]. Scharifker and Hill proposed two distinct regions in I-t transient curve; the peak associated to the cathodic current and the decrease in the current by Cottrell equation. The peak represents the summation of nuclei current and the decrease in current is associated to overlapping the diffusion layer by the particles during nucleation. Fig. 3 shows the plot of an experimental results and the theoretical calculations carried by using equations (3) and (4) for instantaneous and progressive nucleation, respectively to the Cu-In films deposited at −0.7 V (a), −1.0 V (b) and −1.3 V (c).

$$\left(\frac{I}{I_m}\right)^2 = 1.9542\left(\frac{t}{t_m}\right) \times \left\{1 - \exp\left[-1.2564\left(\frac{t}{t_m}\right)\right]\right\}^2 \quad (3)$$

$$\left(\frac{I}{I_m}\right)^2 = 1.2254\left(\frac{t}{t_m}\right) \times \left\{1 - \exp\left[-2.3367\left(\frac{t}{t_m}\right)\right]\right\}^2 \quad (4)$$

where I_m represents the peak current density; t_m is the time of peak current.

The experimental transient curves for growth potentials −0.7 V and −1.0 V exhibits to some extent progressive nucleation fit with a sharper inclined peak, which could be due to the diffusion controlled nucleation process.

For higher cathodic growth potential, −1.3 V, a similar trend was observed in the experimental data for short time (double layer charging) i.e progressive nucleation and later the slow decrease in current close fit to the theoretical curves for the instantaneous nucleation process. The above observation confirms the mixed nucleation process due to the mixed charge-transfer and diffusion controlled mechanism takes place for the sample grown at −1.3 V. A similar explanation on the electrodeposition of for cobalt and platinum is reported [33,34]. The charge transfer reactions, variation in conducting properties of electrode during deposition and variation in precursor concentration in the solution may contribute the deviation of the experimental data from theoretical data.

Fig. 4 depicts the x-ray diffractograms of as-deposited Cu-In intermetallic thin films electrodeposited at (a) −0.7 V, (b) −1.0 V and (c) −1.3 V on to FTO substrates. Polycrystalline thin layers of Cu-In intermetallic layers are deposited from non-aqueous bath for all deposition potentials. The diffraction peaks attributed in XRD

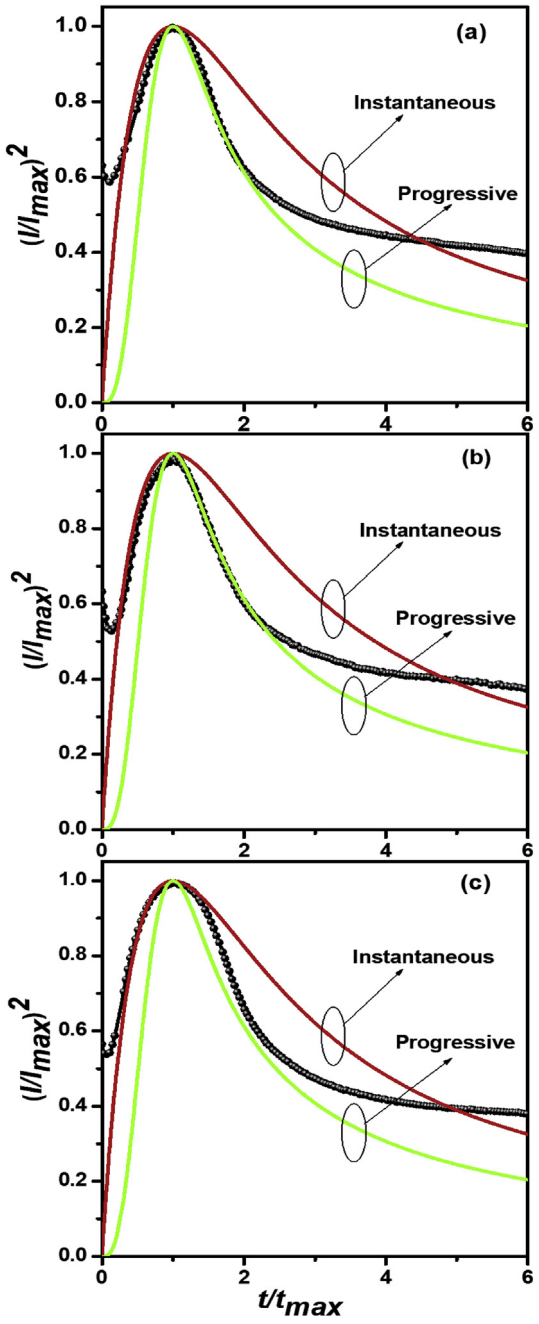

Fig. 3. $(I/I_{max})^2$ versus (t/t_{max}) plots for Cu-In layers deposited at −0.7 V (a), −1.0 V (b) and −1.3 V (c) potentials with corresponding theoretical results obtained for instantaneous and progressive nucleation (continues line).

pattern for the samples deposited at −1.0 V and −1.3 V are agrees well with the standard JCPDF (File No. 41-0883) data of $Cu_{11}In_9$ monoclinic crystal structure. The additional peaks observed for the sample grown at −0.7 V corresponds to $Cu_{16}In_9$ phase (JCPDF File No. 26-0522). The individual metallic Cu and In peaks were not observed in the XRD pattern. The peaks associated to the FTO under layers are marked as solid circles (●).

SEM images of Cu-In layers deposited at various deposition potentials are given in Fig. 5. Films deposited for all three potentials were compact, void-free and well adherent to the substrate. The films grown at potentials, −0.7 V and −1.0 V show granular morphology, Fig. 5a) and b). The grain size was found to be

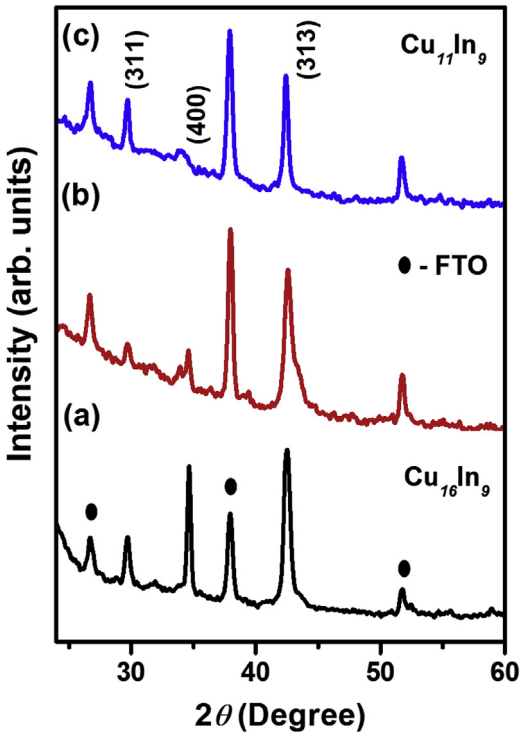

Fig. 4. X-ray diffractogram of Cu-In thin films electrodeposited at −0.7 V (a), −1.0 V (b) and −1.3 V (c).

increased for film deposited at −1.0 V. A mixed, spherical as well as rod like morphology was observed for the Cu-In film deposited at −1.3 V (Fig. 5 c). These SEM results confirm that the deposition potentials play an important role to control the surface morphology. In addition the viscosity of the growth solution and bath temperature can also control the shape and size of the particle. Ethylene glycol is highly viscous, the viscosity is inversely proportional to the diffusion coefficient; therefore the rate of transport of depositing species varies and results in different morphology.

The mixed spherical and dendrites surface morphology (Fig. 5c) at higher deposition potential could be related to the dominating diffusion controlled mechanism. The result obtained from current transient analysis also supports the SEM analyses. Fig. 5 d) represents the plot of atomic composition with respect to deposition potential of Cu-In thin films determined by EDAX analysis. It was observed that the Cu-content decreases and In increases in the deposits upon increasing the growth potentials, which is consistent with the electrochemical behavior of Cu and In (equations (1) and (2)). The above results are in good agreement with XRD analysis.

3.2. Results obtained for selenized Cu-In thin films

The Cu-In thin films deposited at different potentials, −0.7, −1.0 and −1.3 V were selenized in controlled atmosphere to obtain the ternary chalcopyrite phase of $CuInSe_2$. The selenized layers were characterized thoroughly to study the structural, optical, compositional, morphological and optoelectronic properties. Fig. 6 represents the XRD pattern of selenized Cu-In intermetallic layers deposited at −0.7 V (a), −1.0 V (b) and −1.3 V (c). Three prominent reflections, (112), (204/220) and (312)/(116) corresponds to tetragonal crystal structure of CIS were exhibited in all selenized samples. Peaks related to Cu_xS_{1-x} along with CIS reflections were attributed for the Cu-In layers grown at lower cathodic potentials, i. e. −0.7 V and −1.0 V, whereas the selenized Cu-In sample film

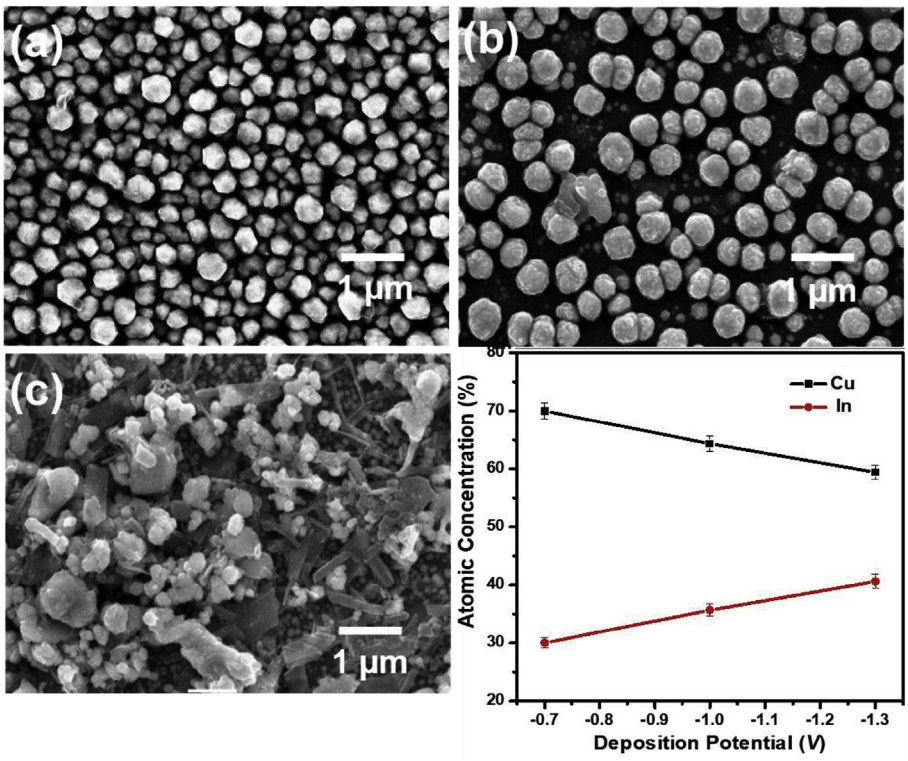

Fig. 5. SEM images of Cu-In thin films electrodeposited at −0.7 V (a), −1.0 V (b), −1.3 V (c) and corresponding plot for atomic concentration versus deposition potential (d).

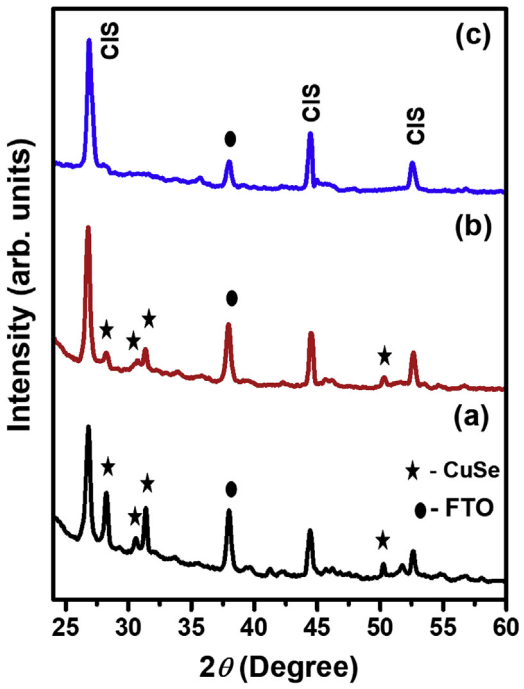

Fig. 6. X-ray diffractogram of selenized Cu-In thin films electrodeposited at −0.7 V (a), −1.0 V (b) and −1.3 V (c). Peaks associated to FTO substrate and CuSe are marked as (•) and (*), respectively.

deposited at −1.3 V exhibited only CIS reflections.

The surface morphology of selenized Cu-In thin films was studied by using SEM analysis. Fig. 7 shows the SEM images of selenized Cu-In thin films prepared at potentials, −0.7 V (a), −1.0 V (b), −1.3 V (c) and the corresponding plot of atomic percentage concentration versus deposition potential is given in Fig. 7d). All selenized films were compact, adherent and densely packed with somewhat irregular shaped morphology. The sample deposited at lower potentials (−0.7 V and −1.0 V) demonstrates the grain size in the range from ~500 nm to l.5 μm, whereas the film obtained at −1.3 V shows slightly large grain growth in the range from ~1 to 2 μm. These homogeneous, well adherent crystalline layers with large clusters are advantageous for the development of high efficiency thin film solar cells. The bulk atomic concentration obtained by EDAX revealed the growth of Cu-rich CIS layers obtained upon selenization of Cu-In samples deposited at lower cathodic potentials, Fig. 7d). Nearly stoichiometric CIS thin films with atomic percentage concentration ~29.7, 24.6 and 45.7 of Cu, In and Se, respectively were obtained for the selenized Cu-In sample deposited at −1.3 V.

Fig. 8 shows the Tauc plot, $(\alpha h\nu)^2$ versus $(h\nu)$ for CIS films obtained upon selenized Cu-In layers deposited at −0.7 V (a), −1.0 V (b) and −1.3 V (c). The energy band gap ~1.06 eV was estimated for CIS layer obtained from Cu-In layer grown at −1.3 V. The value of band gap measured for selenized Cu-In thin films grown at lower cathodic potential were found to be increased, which is proposed due to the presence of secondary phases of Cu_xSe_{1-x} and the small size particles. Indeed, we have observed the peaks associated to Cu_xSe_{1-x} in the selenized layer of Cu-In grown at lower cathodic potentials (−0.7 V and −1.3 V). Two onsets can be clearly seen for the selenized Cu-In alloy thin layers grown at −0.7 V and −1.3 V. A lower band gap ~0.9 eV observed in the sample grown at −1.3 V is proposed due to the deposition of In-rich CIS thin film [35]. It is noteworthy that the In-content in the CIS layer obtained at −1.3 V is more with respect to the layer obtained at −0.7 V and −1.0 V (Fig. 7 (d)). An extra band gap attributed ~1.1 eV in the sample grown at −0.7 V could be associated to the stoichiometric CIS.

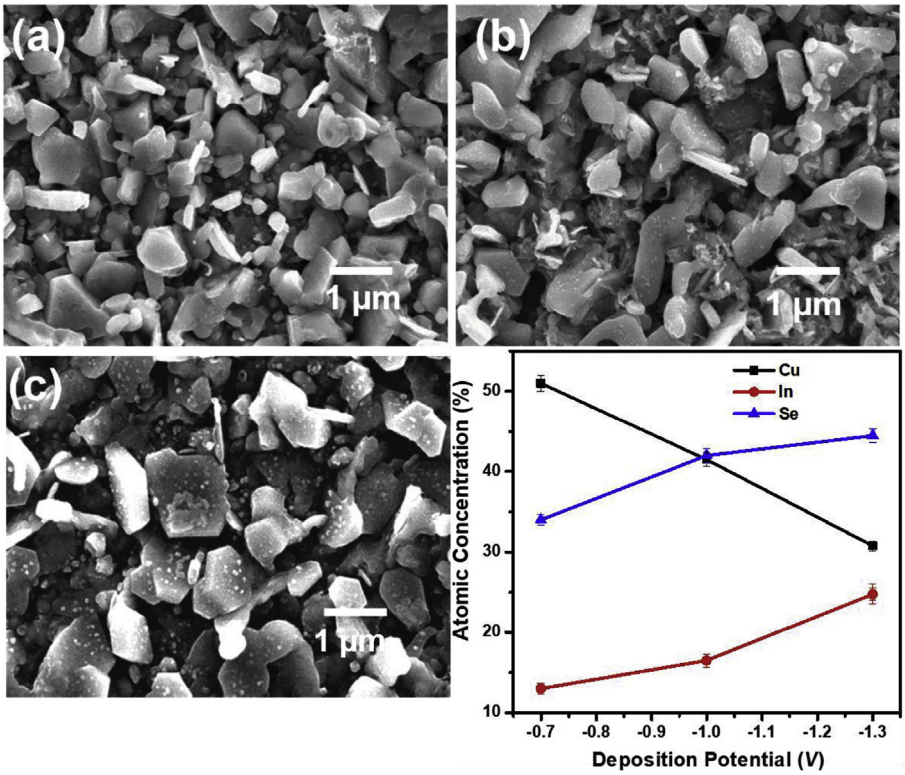

Fig. 7. SEM images of selenized Cu-In thin films (CIS) electrodeposited at -0.7 V (a), −1.0 V (b), −1.3 V (c) and corresponding plot for atomic concentration versus deposition potential (d).

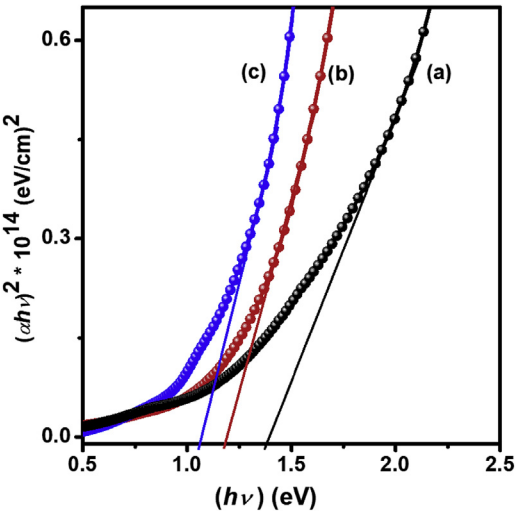

Fig. 8. Plot of $(\alpha h\nu)^2$ versus $(h\nu)$ of the selenized Cu-In thin films deposited at −0.7 V (a), −1.0 V (b) and −1.3 V (c).

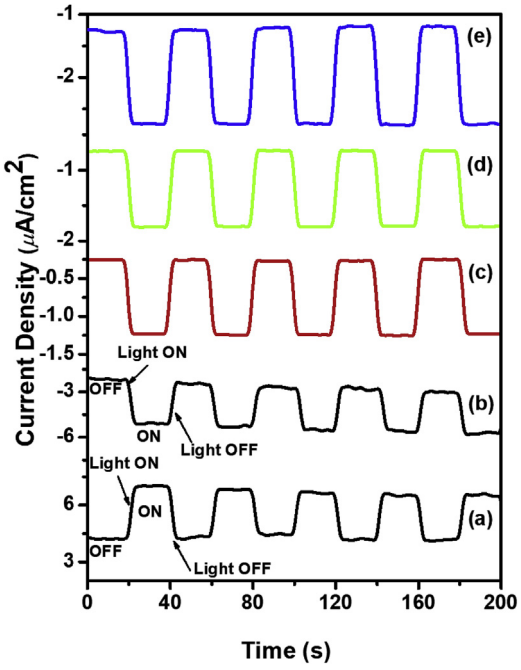

Fig. 9. Photoelectrochemical measurements, photocurrent density verses time for standard n-type Silicon a), p-type Silicon b), selenized Cu-In alloy thin films deposited at −0.7 V (c), −1.0 V (d) and −1.3 V (e).

Photoelectrochemical (PEC) measurements of selenized Cu-In thin films grown at −0.7 (c), −1.0 V (d) and −1.3 V (e) are represented in Fig. 9. The 'n' and 'p'-type standard silicon samples of resistivity 0.05 Ωcm were used as a reference to confirm the direction of photocurrent. The spectra given in Fig. 9a) and b) corresponds 'n' and 'p'-type Silicon sample, respectively. A three electrode system was used to carry the PEC measurements in 1 M KCl electrolyte with a chopped light of intensity 10 mW/cm^2 at room temperature. The direction of photocurrent in PEC measurements by minority charge carries upon illumination gives the information about type of conductivity. All selenized Cu-In alloy samples measured the negative photocurrent and which was

further increased along negative direction demonstrate the p-type conductivity. The photocurrent for the selenized Cu-In alloy samples deposited at −1.0 V and −1.3 V was found to be increased in negative direction as compared to Cu-In films deposited at −0.7 V, which could be associated to stoichiometric growth of layer and also the presence of large particles and absence of unwanted secondary phases.

Fig. 10 shows the Nyquist plots for selenized Cu-In thin films recorded at the frequencies 1 MHz–0.1 mHz deposited at −0.7 V (a), −1.0 V (b) and −1.3 V (c). The equivalent circuit shown in the inset of Fig. 10, which is used to fit the data to calculate the values of series resistance associated to the electrolyte (R_s), the capacitance (C_d) at the electrode-electrolyte interface, the charge transfer resistance (R_{ct}) and Warburg impedance (Z_w). A semicircle in the high-frequency region and a straight line in the low-frequency region can be clearly seen in the Nyquist plots for all three cases. The straight line at low frequency represents the Warburg impedance (Z_w), which is proposed due to the diffusion of ions/electroactive species from the electrolyte to CIS layer. The values of all above estimated parameters are summarized in Table 1. As expected the value of R_s decreases systematically for the selenized Cu-In layer grown at −1.3 V. By measuring the diameter of semicircle at the X-axis the value of R_{ct} is calculated, which was found to be decreased systematically with increasing the deposition potential. C_d represents the capacitance value of the electric double layer formed at the electrode and electrolyte interface. For the selenized Cu-In layer deposited at higher deposition potential measured the large value of C_d.

Based on the above results, a selenized Cu-In layer deposited at −1.3 V was used to prepare the superstrate solar cell structure, FTO/CdS/selenized-Cu-In/Au. A circular metal (Au) contact of diameter 3 mm was prepared by thermal evaporation technique. CdS thin film used as window layer was deposited by chemical bath deposition [30]. To remove the unwanted secondary phases as well as the overgrowth the CIS samples were etched in Br-methanol and NaCN solution prior to make the Au contacts. Fig. 11 illustrates the *J-V* curves measured for dark and illuminated conditions for the final solar cell device at room temperature. The solar cell parameters such as open circuit voltage (V_{OC}), short circuit current (J_{SC}), fill factor (*FF*) and power conversion efficiency (η) measured for typical device under illumination condition are given in Table 2. The efficiency ~5.44% was measured for the above solar cell, which is however low, but can be further improved by optimizing the heat-treatment and etching conditions. The cross-over observed in between dark and illuminated J-V characteristics of solar cell could be associated to the defects present at the interface of CIS/CdS or in absorber layer or in buffer layer [36]. The values of shunt conductance ($G_{D,\ L}$), series resistance ($R_{S\ D,\ L}$), and ideality factor ($A_{D,\ L}$) deduced from the plots of dJ/dV versus V and dV/dJ versus $(J+J_{sc})^{-1}$ under dark and illuminated conditions are tabulated in Table 2. The values of ideality factor and series resistance of solar cell are found to be decreased after illumination. $G_D = 1.1\ mS/cm^2$ and $G_L = 13\ mS/cm^2$ are the values of shunt conductance estimated from the plot dJ/dV versus V at dark and illuminated condition for the CdS/CIS solar cell.

Fig. 12shows the plot of Im(Z) and Re(Z) of a typical CdS/CIS solar cell device at V = 455 mV. In order to quantify the impedance data the results were analyzed by establishing the equivalent circuit which is shown in the inset of Fig. 12. The solid line indicates the fitted data. The only junction formed at the interface between p-CIS and n-CdS was considered and the configured equivalent circuit consists, *Rs*, series resistance (resistance because of bulk and contact resistances) and *Rp*, parallel resistance (resistance due to recombination in the depletion region) and *Co*, the total capacitance (addition of depletion and diffusion capacitances). A semi circular nature was obtained for both the dark and illuminated conditions. The diameter of semicircle represents the value of *Rp*, whereas the displacement from origin on x-axis or the minimum Re(*Z*) at the highest frequency gives the value of *Rs*.

The values of *Rs* ~22 and 12 Ω and *Rp* ~210 and 800 Ω were obtained for dark and illuminated conditions with bias voltage 455 mV. The bulk resistances of CdS and CIS thin layers may contribute the slight increase of *Rs* value [37].

Table 1
Best fit values of R_s, R_{ct}, C_d and Z_w using an equivalent circuit for selenized Cu-In thin films deposited at different deposition potentials.

Deposition potentials (*V*)	R_s (Ω)	R_{ct} (Ω)	C_d (μF)	Z_W (Ω)
−0.7	53.03	6998	2.1	1141
−1.0	49.23	6529	4.5	965
−1.3	33.27	5228	6.1	786

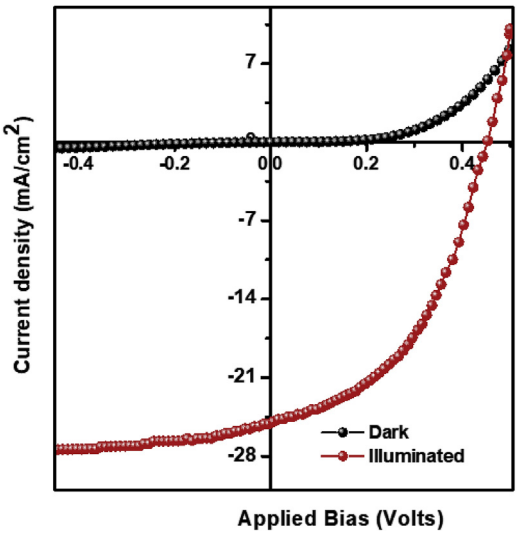

Fig. 11. Dark and illuminated *J-V* curves of FTO/CdS/selenized Cu-In/Au superstrate heterostructure solar cell device. Cu-In layer was electrodeposited at −1.3 V.

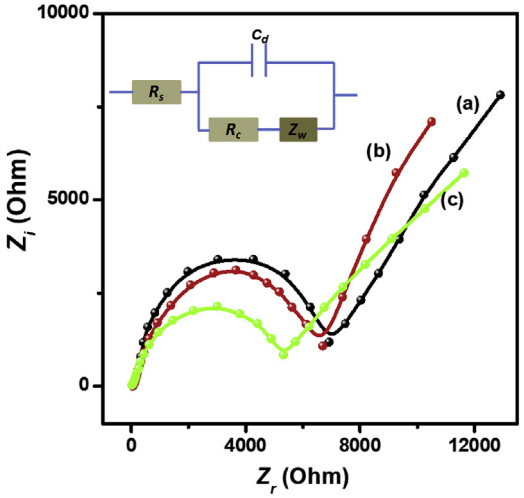

Fig. 10. Nyquist plots for selenized Cu-In thin films deposited at −0.7 V (a), −1.0 V (b) and −1.3 V (c).

Table 2
Solar cell parameters obtained under dark and illuminated conditions.

Cell	V_{OC} (Volts)	J_{SC} (mA/cm^2)	*FF*	Efficiency (η %)	G_D (mS/cm^2)	G_L (mS/cm^2)	$R_{S,D}\Omega$ cm^2	$R_{S,L}\Omega$ cm^2	A_D	A_L
FTO/CdS/Selenized-Cu-In/Au	0.455	26	0.46	5.44	1.1	13	2	0.5	2.1	1.9

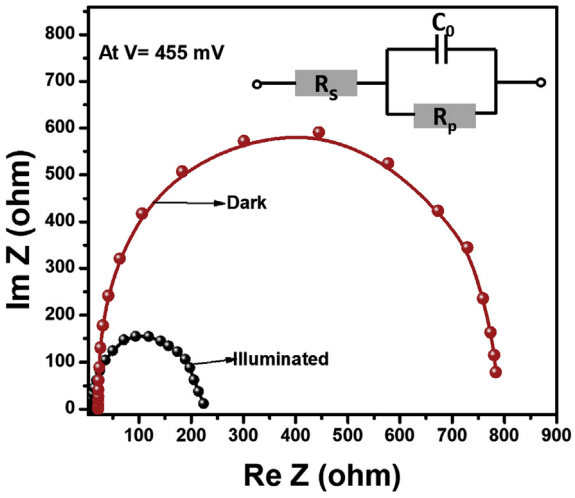

Fig. 12. Impedance spectroscopy measurement of CdS/CIS thin film solar cell at Voc = 455 mV under dark and illuminated conditions.

4. Conclusions

Cu-In layers have been deposited using a low-cost wet electrochemical technique in non-aqueous bath. The layers were selenized in the controlled selenium ambient to obtain the $CuInSe_2$ thin films. A stable, polycrystalline, well adherent intermetallic $Cu_{11}In_9$ thin films with monoclinic crystal structure were obtained at −1.0 and −1.3 V growth potentials. The shape and size of the particle was found to be dependent on the growth potential probably due to the dominating diffusion controlled mechanism. The selenized Cu-In layer sample deposited at −1.3 V measure ~1.06 eV energy band gap with polycrystalline tetragonal chalcopyrite crystal structure of CIS. The photoelectrochemical measurement confirms the growth of p-type material. A selenized Cu-In layer deposited at −1.3 V with CdS window layer measured the power conversion efficiency 5.44%.

Acknowledgements

The financial support received from Department of Science and Technology, New Delhi, India, Grant Ref. No. DST/TM/SERI/FR/124(G) and UPE (II) are gratefully acknowledged. One of the authors PUL is thankful to BARTI for fellowship.

References

[1] http://www.kaneka.co.jp/en/images/topics/1473811995/1473811995_101.pdf%20(accessed%2025%20Octo-ber%202016).
[2] H. Morkoç, S. Strite, G. Gao, M. Lin, B. Sverdlov, M. Burns, J. Appl. Phys. 76 (3) (1994) 1363.
[3] P. Jackson, D. Hariskos, R. Wuerz, O. Kiowski, A. Bauer, T.M. Friedlmeier, M. Powalla, Phys. Status Solidi RRL 9 (1) (2015) 28–31.
[4] M.A. Green, Y. Hishikawa, W. Warta, E.D. Dunlop, D.H. Levi, J.H. Ebinger, A.W.Y. HO-Baillie, Prog. Photovoltaics Res. Appl. 25 (2017) 668–676.
[5] https://www.greentechmedia.com/articles/read/first-solar-hits-record-22-1-conversion-efficiency-for-cdte-solar-cell.
[6] M. Osial, J. Widera, K. Jackowska, J. Solid State Electrochem. 17 (2013) 2477–2486.
[7] J.M. Pearce, N. Podraza, R.W. Collins, M.M. Al-Jassim, K.M. Jones, J. Deng, R. Wronski, J. Appl. Phys. 101 (2007), 114301.
[8] H. Sai, K. Maejima, T. Matsui, T. Koida, M. Kondo, S. Nakao, Y. Takeuchi, H. Katayama, I. Yoshida, Jpn. J. Appl. Phys. 54 (2015), 08KB05.
[9] A.M. Hermanna, C. Gonzaleza, P.A. Ramakrishnan, D. Balzar, N. Popa, P. Rice, C.H. Marshall, J.N. Hilfiker, T. Tiwald, P.J. Sebastian, M.E. Calixto, R.N. Bhattacharya, Sol. Energy Mater. Sol. Cells 70 (2001) 345–361.
[10] C.R. Abernathy, C.W. Bates, A.A. Anani, B. Haba, G. Smestad, Appl. Phys. Lett. 45 (1984) 890–892.
[11] N.B. Chaure, J. Young, A.P. Samantilleke, I.M. Dharmadasa, Sol. Energy Mater. Sol. Cells 81 (2004) 125–133.
[12] P.U. Londhe, A.B. Rohom, M.G. Lakhe, G.R. Bhand, N.B. Chaure, Semicond. Sci. Technol. 31 (11pp) (2016), 125009.
[13] R.N. Bhattacharya, J.F. Hiltner, W. Batchelor, M.A. Contreras, R.N. Noufi, J.R. Sites, Thin Solid Films 361–362 (2000) 396–399.
[14] P.U. Londhe, A.B. Rohom, N.B. Chaure, RSC Adv. 5 (2015) 89635–89643.
[15] A.B. Rohom, P.U. Londhe, N.B. Chaure, Thin Solid Films 642 (2017) 303–310.
[16] J. Yuan, C. Shao, L. Zheng, M. Fan, H. Lu, C. Hao, D. Tao, Vacuum 99 (2014) 196–203.
[17] R. Koutsikou, M. Bouroushian, Electrochim. Acta 178 (2015) 856–870.
[18] R. Ugarte, R. Schrebler, R. Cordova, E.A. Dalchiele, H. Gomez, Thin Solid Films 340 (2000) 117–124.
[19] F.J. Pern, J. Goral, R.J. Matson, T.A. Gessert, R. Noufi, Sol. Cell. 24 (1988) 81–90.
[20] G. Norsworthy, C.R. Eidholm, A. Halaj, V.K. Kapur, R. Roe, B.M. Basol, R. Matson, Sol. Energy Mater. Sol. Cells 60 (2000) 127.
[21] C. Kind, C. Feldmann, A. Quintilla, E. Ahiswede, Chem. Mater. 23 (2011) 5269–5274.
[22] P.P. Prosini, M.L. Addonizio, A. Antonaia, S. Loreti, Thin Solid Films 298 (1996) 191–196.
[23] J. Herrero, J. Ortega, Sol. Energy Mater. Sol. Cells 20 (1990) 53–65.
[24] Y. Cummings, G. Zoppi, I. Forbes, D. Colombara, L.M. Peter, F. Marken, Electrochim. Acta 79 (2012) 141–147.
[25] R.N. Bhattacharya, A.M. Fernandez, Sol. Energy Mater. Sol. Cell. 76 (2003) 331–337.
[26] A.C. Alcanfora, L.P.M. Santosa, D.F. Dias, A.N. Correia, P. Lima-Neto, Electrochim. Acta 235 (2017) 553–560.
[27] P.U. Londhe, A.B. Rohom, R. Fernandes, D.C. Kothari, N.B. Chaure, ACS Sustain. Chem. Eng. 2018 (6) (2018) 4987–4995.
[28] N.G. Dhere, Sol. Energy Mater. Sol. Cells 91 (2007) 1376–1382.
[29] A.M. Fernandez, M.E. Calixto, P.J. Sebastian, S.A. Gamboa, A.M. Hermann, R.N. Noufi, Sol. Energy Mater. Sol. Cells 52 (1998) 423–431.
[30] N.B. Chaure, S. Bordas, A.P. Samantilleke, S.N. Chaure, J. Haigh, I.M. Dharmadasa, Thin Solid Films 437 (2003) 10–17.
[31] A.B. Rohom, P.U. Londhe, N.B. Chaure, J. Electrochem. Soc. 165 (2018) H3051–H3060.
[32] B. Scharifker, G. Hills, Electrochim. Acta 28 (1983) 879.
[33] Y. Yu, Z. Song, H. Ge, G. Wei, L. Jiang, Mater. Res. Innovat. 20 (2015) 280–284.
[34] J.A. Bennett, G.M. Swain, J. Electrochem. Soc. 157 (2010) F89–F95.
[35] S.M. Firoz Hasan, M.A. Subhan, Mannan KhM, Opt. Mater. 14 (2000) 329–336.
[36] K.B. Messaoud, M. Buffi`ere, G. Brammertz, H. ElAnzeery, S. Oueslati, J. Hamon, B.J. Kniknie, M. Meuris, M. Amlouk, J. Poortmans, Prog. Photovoltaics Res. Appl. 23 (2015) 1608–1620.
[37] J. Kneisel, K. Siemer, I. Luck, D. Braunig, J. Appl. Phys. 88 (2000) 5474.